Received: 9 December 2025 | Revised: 25 February 2026 | Accepted: 9 April 2026 | Published online: 30 April 2026

RESEARCH ARTICLE

Journal of Optics and Photonics Research
2026, Vol. 00(00) 1–11
DOI: 10.47852/bonviewJOPR62028736

BON VIEW PUBLISHING

Estimator Algorithms for Determining the Elastic Properties of Chalcogenide Glasses Based on Elemental Composition

Richard A. Loretz[1,*] and Thomas J. Loretz[2]

[1] *Nuclear Physics Consultant, USA*

[2] *Computer Engineering Service, USA*

Abstract: Accurate prediction of the elastic properties of chalcogenide glasses (ChGs) remains a long-standing challenge due to the structural complexity of amorphous networks and the limited availability of reliable mechanical measurements. In this work, we develop a set of numerical estimator algorithms capable of predicting Poisson's ratio, Young's modulus, the Bulk modulus, and the Shear modulus of a ChG solely from its elemental composition. Building on our earlier density-estimator framework, we introduce two composition-based weighting schemes—XC weighting for Poisson's ratio and XMC weighting for the elastic moduli—that incorporate atomic fraction, atomic weight, and coordination number. Element-specific high- and low-concentration endpoint values are found using a reverse Monte Carlo analysis approach and interpolated using a Sigmoid functional form. The resulting estimators were applied to 171 glass compositions spanning 17 ChG families with previously reported elastic properties. Across this dataset, the estimators achieved standard deviations of approximately 2% for Poisson's ratio and less than 5.7% for the elastic moduli. These results show that the elastic properties of ChGs can be predicted with practical accuracy using only elemental composition, enabling pre-melt screening of candidate materials and reducing experimental cost and effort.

Keywords: elastic properties, photonic materials, chalcogenide glass (ChG), machine learning, element-based estimator algorithms

1. Introduction

Chalcogenide glasses (ChGs) occupy a central role in modern photonics and infrared technology due to their broad infrared transparency, high refractive indices, and favorable nonlinear optical behavior. Their utility spans infrared imaging, fiber-based sensing, acousto-optic devices, and integrated photonics. Despite these advantages, ChGs are mechanically softer and more brittle than oxide glasses, making their elastic properties critical determinants of manufacturability, durability, and long-term reliability.

Mechanical behavior in amorphous materials is governed by four fundamental elastic constants: Young's modulus (E), Shear modulus (G), Bulk modulus (K), and Poisson's ratio (ν). These parameters dictate how a glass responds to tensile, compressive, shear, and volumetric stresses, respectively. For ChGs, they influence fiber draw stability, thin-film adhesion, resistance to micro-cracking, pressure-induced refractive index changes, and the ability of optical components to survive thermal cycling or mechanical shock.

In practice:

1) Young's modulus (E) represents the elasticity of the network glass and governs deformation during fiber drawing, molding, and thin-film deposition.
2) Shear modulus (G) correlates strongly with brittleness and fracture susceptibility.
3) Bulk modulus (K) describes compressibility and affects pressure-dependent optical behavior.
4) Poisson's ratio (ν) is a widely used indicator of ductility versus brittleness and is strongly linked to crack resistance and thermal-stress tolerance.

Although these constants are interrelated through well-known isotropic elasticity equations, direct measurement of any of them requires specialized equipment, carefully annealed samples, and sufficient melt mass—conditions that are not always achievable in laboratory-scale ChG research. As a result, researchers often lack mechanical data for many compositions of interest. Our team is actively pursuing ChG atomic bonding and how compositional trends influence optical, electronic, and mechanical properties of the material. In an upcoming article, we will release our new model, which provides better insights into ChG atomic bonding. It will further the theory introduced by Loretz et al. [1] by supplying general equations, which can be used to predict ChG density directly and far more accurately, based solely on composition. In the interim, to address the present gap of the lack of mechanical data in these materials, we employed a subset of our new model strategy to generate estimator algorithms that predict all four elastic constants directly. We introduce two

***Corresponding author:** Richard A. Loretz, Nuclear Physics Consultant, USA. Email: Richard.A.Loretz@comcast.net

© The Author(s) 2026. Published by BON VIEW PUBLISHING PTE. LTD. This is an open access article under the CC BY License (https://creativecommons.org/licenses/by/4.0/).

numerical weighting schemes based on elemental composition and reverse Monte Carlo (RMC)-derived endpoint values:

1) XC weighting for Poisson's ratio (ν), based on atomic fraction and coordination number.
2) XMC weighting for E, K, and G, incorporating atomic fraction, atomic weight, and coordination number.

The choice of XC and XMC weighting was determined by analyzing the datasets and seeing trends in the associated data. Unlike our density research, where there was no overall trend relative to mean coordination number (MCN) [1], measured values of Poisson's Ratio did exhibit an overall trend with XC (which is the same as MCN) for our initial data sources, as shown in Figure 1.

The choice of XMC weighting for the other structural properties was driven by issues we encountered with XC weighting on the other structural properties. Although XC weighting is an improvement over unity weighting, the data showed a nonlinear trend with XC, scatter, and points that did not fit the trend. For instance, see Figure 2(a) for Young's modulus.

Studying the data, we noticed that some of the larger variances were between glass compositions containing lighter elements (e.g., sulfur) versus those containing heavier elements (e.g., selenium, tellurium). Based upon this and our knowledge of physics, we decided to add a mass (M) multiplier to our weighting factor, thus leading to XMC weighting.

When we applied XMC to Young's modulus, the general trend became linear, and the high Young's modulus data point fell within this linear trend, as shown in Figure 2(b). We concluded that XMC weighting would be used in our Young's modulus estimator algorithm since we observed a significant reduction in variance. Similar results were observed for the bulk and shear moduli.

Based upon our interpretation of the accumulated datasets, we determined that a structural properties model might benefit from a Sigmoid-type functional relationship, a mathematical strategy discussed by the authors years earlier while pursuing potential ChG modeling algorithms [2]. For each element, high- and low-concentration endpoint values for the elastic constants are obtained through RMC analysis of published data and interpolated using our empirically determined Sigmoid function. Therefore, our rationale for this approach is based partly upon observed trends in the data and partly on the underlying physics associated with elemental bonding mechanisms.

Our data observations indicated that the element-based quantities were noticeably different when certain elements had a low concentration (doping levels) in the glass versus when the elements had a high abundance in the material matrix. Our data suggested that the elemental values would ramp up (or down) over the low atomic percentage range and reach a constant high concentration asymptotic value. From a physics point of view, for most of the elements, this behavior suggests limited average bonding strengths for an element at low concentration, with rapidly increasing bonding strengths as the element achieves higher concentrations. Once the bonding saturates, the system reaches an asymptotic equilibrium level. Although an argument can be made that each of the other particular elements in the network should have an impact on this bonding, we have chosen to treat their presence as contributing secondary impacts, which we will ignore for our simplified model.

These interpolated elemental contributions are then combined according to the XC or XMC weighting rules to yield the predicted elastic properties of any multicomponent ChG.

We have been using RMC analysis as a tool following the same basic script. The optimization procedure is to determine a

Figure 1
Poisson's ratio vs XC weighting

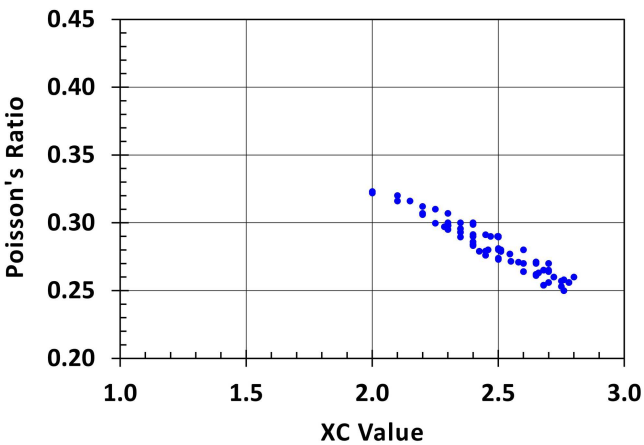

Figure 2
(a) Young's modulus vs XC weighting and (b) Young's modulus vs XMC weighting

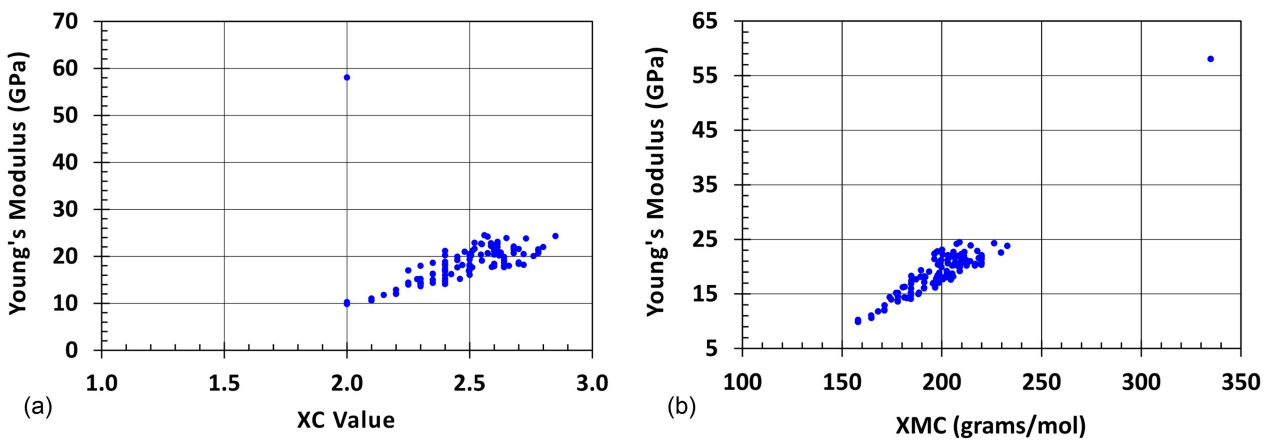

consistent set of high and low elemental constants that reduce the variance between the calculated and measured quantity of interest (ν, E, K, or G) to an acceptable level over the training set of glass compositions.

Before we began the RMC analysis, there was one set of endpoints that could be set by definition. The high concentration end point values for each of the four structural properties for selenium (Se) can be equated to the measured structural properties for bulk fully annealed vitreous (100%) selenium. The advantage of doing this is that it establishes an anchor for each of the structural properties that all other endpoints evolve from during the subsequent RMC iterations rather than having all endpoints variable during the analysis.

The general objective function for the RMC is:

$$\chi^2 = \frac{1}{\mathrm{K}-1}\sum_{\mathrm{k}=1}^{\mathrm{K}}[\mathrm{Q}(\mathrm{Calc_k}) - \mathrm{Q}(\mathrm{Meas_k})]^2 \tag{1}$$

where K is the number of training glass compositions and Q is one of the structural properties.

The training set of glass compositions can be further divided by the elements that they contain. The RMC can be performed for each element over the set of compositions that contain that element. The objective functions are:

$$\chi_{\mathrm{i}}^2 = \frac{1}{\mathrm{K_i}-1}\sum_{\mathrm{k_i}=1}^{\mathrm{K_i}}[\mathrm{Q}(\mathrm{Calc_{k_i}}) - \mathrm{Q}(\mathrm{Meas_{k_i}})]^2 \tag{2}$$

where K_i is the number of glass compositions that contain element i.

Notice that $K \neq \sum_i K_i$ and $\chi^2 \neq 1/(K-1)\sum_i(K_i-1)\chi_i^2$. Since the majority of evaluated glass compositions are composed of multiple elements, the compositions are used multiple times as the elements are repetitively evaluated. By minimizing the χ_i^2 to acceptable levels, the overall goal of reducing the value of χ^2 is simultaneously achieved. One constraint is to ensure the constants remain physical (i.e., positive and reasonable relative to the particular structural property) as the iterations proceed. Random numbers are used to determine the element to be evaluated and whether the high or low limit will be changed by a randomly chosen +/− for evaluation (except selenium, where only the low limit constant will be updated). If the change reduces χ_i^2, the change is accepted. If the change increases χ_i^2, the change is rejected. The RMC analysis is repeated until a consistent set of constants is determined with acceptable χ_i^2 values.

After the constants were determined from our subset of the glass compositions, we evaluate the overall performance of our estimator algorithms using 171 glass compositions drawn from 17 ChG families, representing one of the broadest cross-family comparisons of elastic properties to date. The resulting predictions show strong agreement with reported measurements, with standard deviations (s) about 2% for Poisson's ratio and less than 5.7% for the moduli.

While we believe our estimator algorithms are novel and provide elastic property values that are quite reasonable, we recognize that advances in artificial intelligence and machine learning may lead us or others to algorithms that provide greater accuracy. This may be accomplished by either refining the physics of our basic approach or replacing it with something more innovative. We note that machine learning research for predicting glass properties is actively being addressed by others in the glass science field [3–23].

1.1. Relationships between E, G, K, and ν

Equations exist that allow for the calculation of any one of these elastic constants if two others are known. For homogeneous and isotropic materials, the mathematical relationship between Young's modulus (E), Shear modulus (G), and Poisson's ratio (ν) is:

$$\mathrm{E} = 2\mathrm{G}(1+\nu) \tag{3}$$

For homogeneous and isotropic materials, the mathematical relationship between Young's modulus (E), Bulk modulus (K), and Poisson's ratio (ν) is:

$$\mathrm{E} = 3\mathrm{K}(1-2\nu) \tag{4}$$

For homogeneous and isotropic materials, the mathematical relationship between Shear modulus (G), Bulk modulus (K), and Poisson's ratio (ν) is:

$$\mathrm{G} = \frac{3\mathrm{K}\,(1-2\nu)}{2\,(1+\nu)} \tag{5}$$

Throughout this study, we assumed that the glass compositions evaluated were truly in a supercooled phase and contained no unavoidable nucleation or crystallization. We also assumed that all glass materials were reasonably annealed and did not contain excessive internal flaws or defects. Various sources provided the reported elastic properties for the 171 ChG compositions evaluated in this paper [DA01–DA08, 24–40].

The glass families used in our study are provided in Table 1. The 12 elements used in our study are Ge, As, Se, Sb, S, Te, Si, Pb, La, Ga, In, and Zn. The basic data associated with these elements are provided in Table 2. The atomic weight [Mi] and the coordination number [Ci] for each of the elements are included in the table. [Ci] represents the number of electron bonds in which each can participate. As will be developed in the next section, the quantity [Mi] x [Ci] will play a key role in the weighting scheme employed for estimating the values for Young's modulus, Bulk modulus, and Shear modulus.

2. Estimator Formulations

Predicting elastic properties from elemental composition requires a framework that captures how each constituent element

Table 1
Chalcogenide glass families used in this study

Compositional family				
Vitreous Se	Ge–As–Se	Ge–As–S	Ge–Sb–Se	Zn–Se
Ge–As–Se–Te	Ge–Si–Sb–Te	Ge–Si–As–Te	Ga–La–S	
As–Se	Ge–Sb–S	Ge–Se	As–Sb–Se	
As–S	Ge–S	Ge–Ga–Se–Pb	Ge–Ga–Se–In	

Table 2
Basic data associated with the elements used in this study

Periodic element	Atomic weight [M_i] (gm/mol)	Coordination number [C_i]	Weighting [M_i] x [C_i] (gm/mol)
Ge	72.63	4	290.52
As	74.92	3	224.76
Se	78.97	2	157.94
Sb	121.76	3	365.28
S	32.06	2	64.12
Te	127.60	2	255.20
Si	28.09	4	112.36
Ga	69.72	3	209.16
La	138.91	3	416.73
Pb	207.20	2	414.40
In	114.82	3	344.46
Zn	65.38	2	130.76

contributes to the overall mechanical response of the amorphous network. In this section, we introduce two weighting schemes—XC weighting for Poisson's ratio and XMC weighting for the elastic moduli—along with the interpolation method used to determine element-specific contributions at arbitrary concentrations.

These formulations build directly on our earlier density-estimator methodology, with the key addition of coordination number as a structural weighting factor.

2.1. Estimator for Poisson's ratio (ν)

Several weighting strategies were evaluated for predicting Poisson's ratio from composition. The formulation that produced the most accurate results across the 171-composition dataset is:

$$\nu = \frac{\sum_i X_i \ \text{x} \ [C_i] \text{x} \ \nu_i \ (X_i)}{\sum_i X_i \ \text{x} [C_i]} \tag{6}$$

Where:

1) X_i = atomic fraction of element
2) C_i = coordination number of element
3) $\nu_i(X_i)$ = elemental Poisson's ratio contribution at concentration X_i

We refer to this as XC weighting, since only the atomic fraction and coordination number determine the weighting. Coordination number appears naturally in the RMC analysis as a factor that scales the influence of each element on the network's deformation behavior, without invoking assumptions about covalent bonding dominance.

1) **Elemental endpoint values**

For each element, two fixed endpoint values are defined:

a. a low-concentration limit (0% atom fraction)
b. a high-concentration limit (100% atom fraction)

These values, derived from RMC analysis of published elastic-property data, are listed in Table 3. They represent the intrinsic contribution of each element to Poisson's ratio when present from trace to dominant amounts.

2) **Sigmoid interpolation**

To obtain $\nu_i(X_i)$ at intermediate concentrations, first, we interpolate between the low and high endpoints using a Sigmoid function:

$$\text{Sigmoid} = 2 \times \left\{ \left[\frac{1}{1 + e^{-(7.5788 \text{ x Atom Fraction})}} \right] - 0.5 \right\} \tag{7}$$

Table 3
Fixed set of high and low elemental values for elastic constants

Element \ Atm %	Poisson's ratio (ν)		Young's modulus (E)		Bulk modulus (K)		Shear modulus (G)	
	Low	High	Low	High	Low	High	Low	High
Ge	0.265	0.197	19.7	32.0	24.5	16.5	7.0	12.7
As	0.250	0.293	23.5	24.9	27.8	19.9	8.1	10.0
Se	0.180	0.323	3.0	9.9	2.0	7.8	5.0	3.8
Sb	0.220	0.242	31.5	26.3	23.0	17.0	14.3	6.5
S	0.503	0.300	0.04	0.01	0.08	1.2	0.12	0.04
Te	0.194	0.271	9.6	19.0	8.7	11.9	3.0	9.0
Si	0.250	0.234	35.0	12.0	4.0	6.0	5.6	5.0
Pb	0.300	0.284	8.0	82.9	49.0	65.1	25.3	30.7
La	0.022	0.035	110	117	54.0	74.4	49.0	52.0
Ga	0.210	0.227	43.3	62.7	46.0	44.0	22.0	16.0
In	0.200	0.220	40.0	48.0	27.0	35.0	10.0	15.0
Zn	0.219	0.230	133	138	95.1	104	51.5	53.0

This function provides a smooth transition between endpoint values and reflects the nonlinear manner in which elemental contributions evolve with concentration.

And then, the interpolated elemental Poisson's ratio is:

$$\nu_i(X_i) = \nu_i(\text{low conc}_i) + \text{Sigmoid} \times (\nu_i(\text{high conc}) - \nu_i(\text{low conc})) \tag{8}$$

This formulation captures the concentration-dependent behavior observed in experimental datasets and ensures continuity across multicomponent systems.

Figure 3 (based on the solution of Equation (7)) shows the Sigmoid shape (low to high concentration).

Figure 3
Sigmoid functional form used in this study

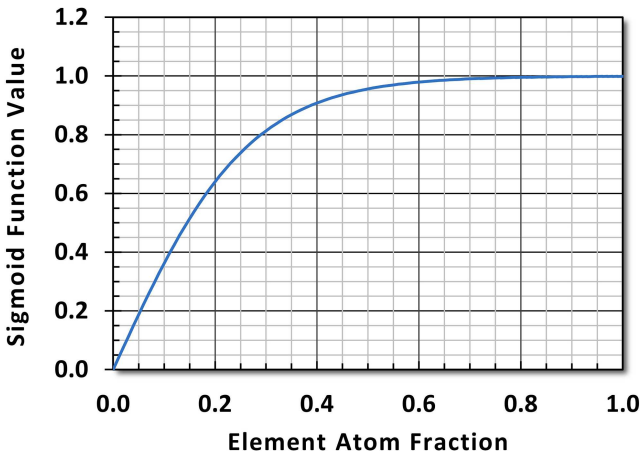

2.2. Estimators for Young's modulus, Bulk modulus, and Shear modulus

Several different weighting formulations were also investigated for estimating the values for the various structural moduli. The schemes that seem to work best are shown in Equations (9)–(11).

$$E = \frac{\sum_i X_i \times ([M_i] \times [C_i]) \times E_i(X_i)}{\sum_i X_i \times ([M_i] \times [C_i])} \tag{9}$$

$$K = \frac{\sum_i X_i \times ([M_i] \times [C_i]) \times K_i(X_i)}{\sum_i X_i \times ([M_i] \times [C_i])} \tag{10}$$

$$G = \frac{\sum_i X_i \times ([M_i] \times [C_i]) \times G_i(X_i)}{\sum_i X_i \times ([M_i] \times [C_i])} \tag{11}$$

Where:

1) $[M_i]$ is the atomic weight of the element i,
2) $E_i(X_i)$ is an elemental value for Young's modulus that depends on the quantity of the element used and is explained below,
3) $K_i(X_i)$ is an elemental value for the Bulk modulus that depends on the quantity of the element used and is explained below, and
4) $G_i(X_i)$ is an elemental value for the Shear modulus that depends on the quantity of the element used and is explained below.

We refer to these weighting schemes for the moduli values collectively as "XMC" weighting, as an element's atom fraction $[X_i]$, molecular weight $[M_i]$, and coordination number $[C_i]$ are used to determine the weighting. The authors have utilized our RMC [1] approach to determine a fixed set of elemental Young's moduli, Bulk moduli, and Shear moduli values that can be interpolated to evaluate the $E_i(X_i)$, $K_i(X_i)$, and $G_i(X_i)$ terms. These values are provided in Table 3. The interpolation scheme for each element uses our Sigmoid function weighting described above. The governing equations are:

$$E_i(X_i) = E_i(\text{low conc}_i) + \text{Sigmoid x}(E_i(\text{high conc}) - E_i(\text{low conc})) \tag{12}$$

$$K_i(X_i) = K_i(\text{low conc}_i) + \text{Sigmoid x}(K_i(\text{high conc}) - K_i(\text{low conc})) \tag{13}$$

$$G_i(X_i) = G_i(\text{low conc}_i) + \text{Sigmoid x}(G_i(\text{high conc}) - G_i(\text{low conc})) \tag{14}$$

2.3. Summary of the estimator framework

The complete estimator system consists of:

1) XC weighting for Poisson's ratio (ν)
2) XMC weighting for E, K, and G
3) RMC-derived elemental endpoint values (Table 3)
4) Sigmoid interpolation to obtain concentration-dependent elemental contributions

This framework is general, requires only elemental composition as input, and is applicable to any multicomponent ChG containing the elements listed in Table 2.

3. Chalcogenide Glass Dataset and Estimator Performance

To evaluate the accuracy and generality of the proposed estimator algorithms, we applied them to a dataset of 171 ChG compositions drawn from 17 distinct compositional families. These families span a broad range of structural chemistries, including binary, ternary, and quaternary systems based on Ge, As, Se, S, Sb, Te, Si, Ga, La, In, Pb, and Zn. Table 1 lists the families included in this study.

As explained earlier, elastic property measurements for these compositions were obtained from published sources [DA01–DA08, 24-40]. Because elastic constants are often measured on small-mass melts (typically <50 g), reported values can exhibit nontrivial scatter due to sample preparation, annealing conditions, and instrument limitations. Despite these challenges, the dataset provides a sufficiently diverse and representative basis for validating the estimator framework.

For each composition, the four elastic constants—Poisson's ratio (ν), Young's modulus (E), Bulk modulus (K), and Shear modulus (G)—were calculated using the XC or XMC weighting schemes and the interpolated elemental contributions described in Section 2. These calculated values were then compared directly to the reported measurements.

3.1. Poisson's ratio (ν)

Figure 4 (based on the analysis of Table 3 and Equation (6)) compares the calculated and measured Poisson's ratios for all compositions with available data. The estimator exhibits strong agreement with reported values:

1) Standard deviation: 2.02%
2) Typical scatter: within ±4.6% (≈2.3σ)

The narrow distribution of deviations demonstrates that Poisson's ratio is particularly well captured by the XC weighting scheme, reflecting the strong correlation between coordination-weighted composition and deformation coupling behavior in ChGs.

3.2. Young's modulus (E)

Figure 5 (based on the analysis of Table 3 and Equation (9)) shows the comparison between calculated and measured Young's modulus values. Across the dataset:

1) Standard deviation: 5.24%
2) Typical scatter: within ±11.7% (≈2.2σ)

Given the known variability in experimental E measurements for small-batch ChGs, this level of agreement indicates that Equation (7), which uses the XMC numerical weighting scheme, effectively captures the composition-dependent elasticity of the amorphous network.

3.3. Bulk modulus (K)

Figure 6 (based on the analysis of Table 3 and Equation (10)) presents the comparison for Bulk modulus. The estimator again performs well:

1) Standard deviation: 4.74%
2) Typical scatter: within ±10.8% (≈2.3σ)

The relatively low scatter suggests that volumetric compressibility is strongly governed by elemental mass and coordination contributions, both of which are central to the XMC weighting formulation.

3.4. Shear modulus (G)

Figure 7 (based on the analysis of Table 3 and Equation (11)) compares calculated and measured Shear modulus values. Among

Figure 4
Poisson's ratio XC-weighted analysis

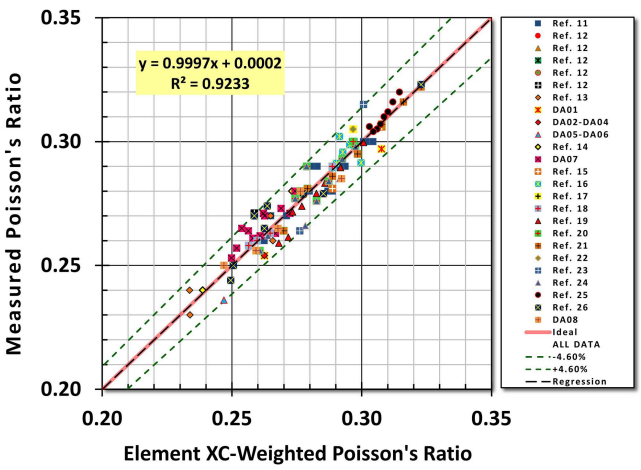

Figure 5
Young's modulus XMC-weighted analysis (with magnification insert for majority zone)

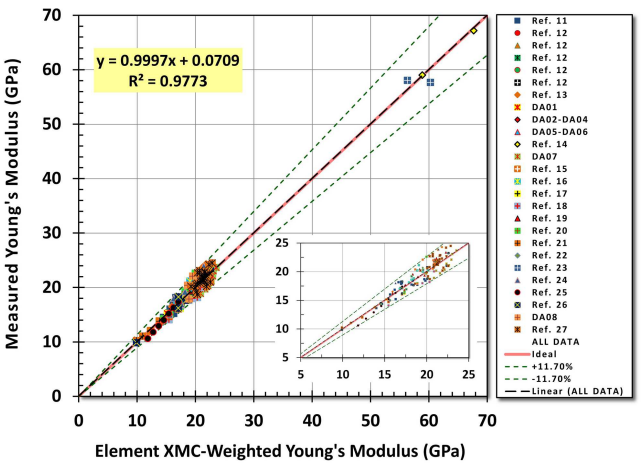

Figure 6
Bulk modulus XMC-weighted analysis (with magnification insert for majority zone)

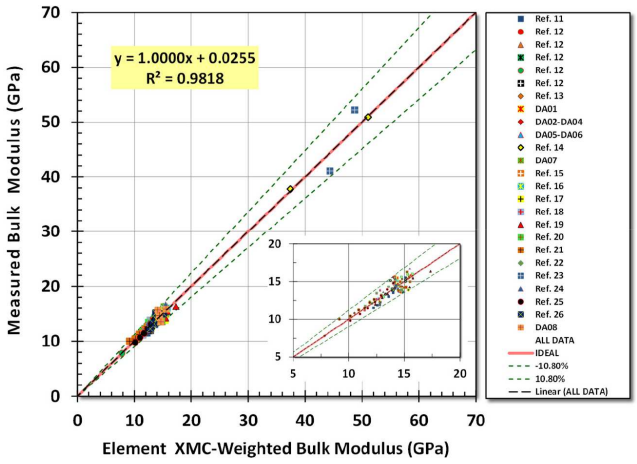

Figure 7
Shear modulus XMC-weighted analysis (with magnification insert for majority zone)

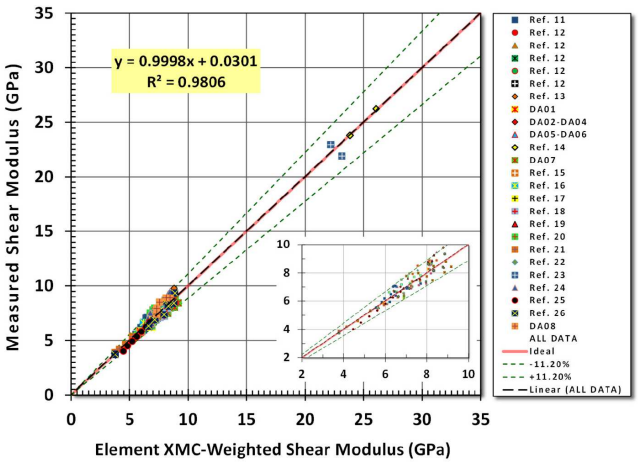

Table 4
Summary of estimator accuracy across all 171 compositions

Elastic property	Weighting scheme	Standard deviation (%)	Typical scatter (%)
Poisson's ratio (n)	XC	2.02	± 4.6
Young's modulus (E)	XMC	5.24	± 11.7
Bulk modulus (K)	XMC	4.74	± 10.8
Shear modulus (G)	XMC	5.70	± 11.2

the three moduli, G is typically the most sensitive to structural defects and micro-cracking, yet the estimator still achieves:

1) Standard deviation: 5.7%
2) Typical scatter: within ±11.2% (≈1.97σ)

This performance indicates that the estimator captures the essential composition-dependent factors governing resistance to shear deformation in ChGs.

3.5. Summary of estimator accuracy

The results of Table 4 demonstrate that the estimator algorithms provide practically useful predictions across a wide range of compositions and structural chemistries. The accuracy achieved is well within the variability expected from experimental measurements of small-mass ChG melts, indicating that the estimators are robust and broadly applicable.

4. Discussion

The estimator algorithms developed in this work demonstrate that the elastic properties of ChGs can be predicted with practical accuracy using only elemental composition. This is a significant result, given the inherent challenges associated with measuring elastic constants in small-batch ChG melts and the wide variability in reported values across the literature. The performance of the estimators—standard deviations of approximately 2% for Poisson's ratio and less than 5.7% for Young's, Bulk, and Shear moduli—indicates that the underlying weighting schemes capture the essential physics governing mechanical behavior in these amorphous networks.

A key strength of the approach lies in the use of element-specific endpoint values derived from RMC analysis. These endpoints encode the intrinsic mechanical influence of each element in both dilute and dominant concentration limits, allowing the estimator to adapt naturally across diverse compositional families. The Sigmoid interpolation ensures smooth transitions between these limits and reflects the nonlinear manner in which structural contributions evolve with concentration. Together, these components provide a flexible yet physically grounded framework for predicting elastic properties across a broad range of ChG chemistries.

The distinction between the XC weighting used for Poisson's ratio and the XMC weighting used for the elastic moduli is also noteworthy. Coordination number alone is sufficient for predicting ν, consistent with its role as a measure of deformation in directions perpendicular to the loading. In contrast, the moduli depend strongly on both atomic mass and bonding capacity, which is reflected in the inclusion of the [MiCi] product as a numerical weighting contributor in the XMC formulation. This separation of weighting schemes emerged directly from the RMC analysis and highlights the importance of treating Poisson's ratio and the moduli as structurally distinct quantities.

Importantly, although the coordination number appears in both weighting schemes, its use here should not be interpreted as support for the MCN theory. MCN theory assumes that ChG networks are dominated by covalent bonding and that a single average coordination value can predict physical properties. Our earlier work has shown that most ChGs are not governed primarily by covalent bonds but instead exhibit a complex mixture of van der Waals (vdW), covalent, and metastable bonding interactions. The coordination number in our estimators serves only as a scaling factor that improves the weighting of elemental contributions; it does not imply any assumptions about the underlying bonding character. Consistent with this, we find no meaningful correlation between MCN and the elastic moduli across the 171 compositions studied.

The estimator performance is also influenced by the quality of the underlying experimental data. Elastic property measurements for ChGs are often performed on melts of limited mass, typically less than 50 grams, and are sensitive to annealing conditions, sample geometry, and instrument calibration. Variations of ±10% in reported values are common. In this context, the estimator deviations observed in this study fall well within the expected experimental uncertainty, suggesting that the algorithms are capturing the true composition-dependent trends rather than overfitting to noisy data.

Looking forward, the availability of additional high-quality elastic property measurements—particularly for underrepresented compositional families—would further refine the elemental endpoint values and improve estimator accuracy. Moreover, advances in machine learning may offer complementary insights by identifying subtle nonlinear relationships or higher-order interactions not captured by the current weighting schemes. Several groups have already begun exploring data-driven approaches to predicting glass properties, and the framework presented here provides a physically interpretable foundation that could be integrated with such methods.

Overall, the results of this study demonstrate that the elastic properties of ChGs can be reliably estimated from composition alone, enabling researchers to evaluate candidate materials before melting and testing. This capability reduces experimental cost, accelerates materials discovery, and provides a unified, composition-based framework for understanding mechanical behavior across a wide range of ChG systems.

5. Worked Examples

To illustrate the practical use of the estimator algorithms, we present two representative examples drawn from the Ge–As–Se and As–Se ChG families. Each example demonstrates how the XC and XMC weighting schemes, together with the Sigmoid-interpolated elemental endpoint values, are used to compute Poisson's ratio, Young's modulus, Bulk modulus, and Shear modulus directly from composition.

All elemental constants used in these examples are taken from Table 3, and all Sigmoid values are computed using Equation (5).

Example 1:
$Ge_{15}As_{10}Se_{75}$ (Measured data source: [24])
Step 1: Table 5 summarizes the compositional and basic data employed in Example 1.

Table 5
Composition and elemental parameters

Element	Atom fraction (X_i)	Atomic weight M_i (gm/mol)	Coordination C_i	M_iC_i
Ge	0.15	72.63	4	290.52
As	0.10	74.92	3	224.76
Se	0.75	78.97	2	157.94

Step 2: Sigmoid values
Using Equation (7):
Sigmoid(0.15) = 0.514
Sigmoid(0.10) = 0.362
Sigmoid(0.75) = 0.993

Step 3: Interpolated elemental contributions
Using Equations (8), (12)–(14):
Poisson's ratio contributions
Ge: 0.265 + 0.514(0.197 − 0.265) = 0.230
As: 0.250 + 0.362(0.293 − 0.250) = 0.266
Se: 0.180 + 0.993(0.323 − 0.180) = 0.322

Table 6 provides the interpolated moduli contributions by element using Equations (12)–(14).

Table 6
Moduli contributions (GPa)

Element	$E_i(X_i)$	$K_i(X_i)$	$G_i(X_i)$
Ge	26.03	20.39	9.93
As	24.01	24.94	8.79
Se	9.86	7.77	3.78

Step 4: Compute Poisson's ratio (XC weighting, Equation (6))

$$\nu = \frac{[(0.15)(4)(0.230) + (0.10)(3)(0.266) + (0.75)(2)(0.322)]}{[(0.15)(4) + (0.10)(3) + (0.75)(2)]} = 0.292$$

Evaluation:
Measured value: 0.290
Difference: 100 × (Calculated – Measured)/Measured = 0.68%

Step 5: Compute elastic moduli (XMC weighting, Equations (9)–(11), respectively)

$$E = \frac{[(0.15)(290.52)(26.03) + (0.10)(224.76)(24.01) + (0.75)(157.94)(9.86)]}{[(0.15)(290.52) + (0.10)(224.76) + (0.75)(157.94)]} = 15.4$$

Young's Modulus
E = 15.4 GPa
Measured: 15.3 GPa
Difference: 100 × (Calculated – Measured)/Measured = 0.67%

$$K = \frac{[(0.15)(290.52)(20.39) + (0.10)(224.76)(24.94) + (0.75)(157.94)(7.77)]}{[(0.15)(290.52) + (0.10)(224.76) + (0.75)(157.94)]} = 12.84$$

Bulk Modulus
K = 12.84 GPa
Measured: 12.27 GPa
Difference: 100 × (Calculated – Measured)/Measured = 4.6%

$$G = \frac{[(0.15)(290.52)(9.93) + (0.10)(224.76)(8.79) + (0.75)(157.94)(3.78)]}{[(0.15)(290.52) + (0.10)(224.76) + (0.75)(157.94)]} = 5.84$$

Shear Modulus
G = 5.84 GPa
Measured: 5.92 GPa
Difference: 100 × (Calculated – Measured)/Measured = –1.32%

Example 2:
$As_{30}Se_{70}$ (Measured data source: [38])
Step 1: Table 7 summarizes the compositional and basic data employed in Example 2.

Table 7
Composition and elemental parameters

Element	Atom fraction (X_i)	Atomic weight M_i (gm/mol)	Coordination (C_i)	M_iC_i
As	0.30	74.92	3	224.76
Se	0.70	78.97	2	157.94

Step 2: Sigmoid values
Sigmoid(0.30) = 0.813
Sigmoid(0.70) = 0.990

Step 3: Interpolated elemental contributions
Poisson's ratio contributions
As: 0.250 + 0.813(0.293 − 0.250) = 0.285
Se: 0.180 + 0.990(0.323 − 0.180) = 0.322

Table 8 provides the interpolated moduli contributions by element using Equations (12)–(14).

Table 8
Moduli contributions (GPa)

Element	$E_i(x_i)$	$K_i(X_i)$	$G_i(X_i)$
As	24.64	21.38	9.65
se	9.84	7.75	3.78

Step 4: Compute Poisson's ratio

$$\nu = \frac{[(0.30)(3)(0.285) + (0.70)(2)(0.322)]}{[(0.30)(3) + (0.70)(2)]} = 0.308$$

Evaluation:
Measured: 0.307
Difference: 100 × (Calculated – Measured)/Measured = 0.3%

Step 5: Compute elastic moduli
Young's Modulus

$$E = \frac{[(0.30)(224.76)(24.64) + (0.70)(157.94)(9.84)]}{[(0.30)(224.76) + (0.70)(157.94)]} = 15.45$$

E = 15.45 GPa
Measured: 15.20 GPa
Difference: 100 × (Calculated − Measured)/Measured = 1.59%

$$K = \frac{[(0.30)(224.76)(21.38) + (0.70)(157.94)(7.75)]}{[(0.30)(224.76) + (0.70)(157.94)]} = 12.91$$

Bulk Modulus
K = 12.91 GPa
Measured: 13.13 GPa
Difference: 100 × (Calculated − Measured)/Measured = −1.65%

$$G = \frac{[(0.30)(224.76)(9.65) + (0.70)(157.94)(3.78)]}{[(0.30)(224.76) + (0.70)(157.94)]} = 6.00$$

Shear Modulus
G = 6.00 GPa
Measured: 5.82 GPa
Difference: 100 × (Calculated − Measured)/Measured = 3.10%
Summary of Examples
These two examples demonstrate:

1) The estimator algorithms reproduce measured elastic properties with very good accuracy.
2) Deviations are typically below the experimental uncertainty expected for small-mass ChG melts.
3) The XC and XMC weighting schemes work well across different families and bonding chemistries.
4) The Sigmoid interpolation provides smooth, physically reasonable transitions between elemental endpoint values.
5) Together, these examples illustrate how the estimator framework can be applied to any multicomponent ChG containing the elements listed in Table 2.

6. Conclusions

This study demonstrates that the elastic properties of ChGs—Poisson's ratio, Young's modulus, Bulk modulus, and Shear modulus—can be predicted with practical accuracy using only the elemental composition of the glass. By combining RMC-derived elemental endpoint values with composition-based weighting schemes (XC for Poisson's ratio and XMC for the elastic moduli), we developed a unified estimator framework capable of reproducing measured elastic constants across a broad range of ChG families.

Application of the estimators to 171 compositions from 17 distinct ChG families yielded strong agreement with reported measurements, with standard deviations of approximately 2% for Poisson's ratio and less than 5.7% for the elastic moduli. These deviations fall well within the experimental variability typically associated with small-mass ChG melts, indicating that the estimators capture the essential composition-dependent trends governing mechanical behavior in these materials.

A key advantage of this approach is that it requires no structural assumptions about bonding character or network topology. Although the coordination number appears in the weighting schemes, its use is purely empirical and does not imply support for the MCN theory. Consistent with our earlier findings, we observe no meaningful correlation between MCN and the elastic moduli across the compositions studied. Instead, the estimator framework relies on elemental contributions derived directly from experimental data, making it broadly applicable to multicomponent systems with diverse bonding environments.

The ability to estimate elastic properties from composition alone provides a valuable tool for researchers and glass designers. It enables pre-melt screening of candidate materials, reduces experimental cost and effort, and accelerates the development of new ChG compositions for infrared optics, photonics, and related technologies. As additional high-quality elastic property data become available, the elemental endpoint values can be refined further, and integration with modern machine learning techniques may offer additional improvements.

Historical models based on Phillips–Thorpe (P–T) constraint theory predict a sharp transition to "rigidity" and a corresponding drop in Poisson's ratio (ν) as coordination increases. Traditional ChG atomic bonding models assume a 3D covalent network that becomes "rigid" at a coordination number $r \cong 2.4$. It is a theory which states that ChGs are governed predominantly—if not completely—by continuous 3D covalent cross-linking as opposed to intermolecular vdW interactions. The results of our elastic properties research contained within this article contradict (P–T) theory by revealing mechanical "softness" in As-rich As–Se systems and Ge-rich ternary systems. This new evidence further supports our vdW predominance theory [1]. Macroscopic elastic response is limited by the weak, vdW structural links. Arguably, we envisage these links to be vdW "intermolecular gaps" found between layers of covalent bond motifs. More importantly, this support offers a physical explanation for many physical behaviors that covalent models struggle to justify, especially density. ChGs are actually held together by the weaker vdW forces between molecular cluster or chain motifs. Thus, these amorphous materials present a "rigidity," which is far more fluid and which helps to explain why many ChGs exhibit intermediate-to-fragile behavior rather than the extreme "strength" of a 3D network like amorphous SiO_2. VdW bonds are significantly more sensitive to thermal fluctuations than covalent bonds. High sensitivity translates directly into a higher fragility index, as the liquid's viscosity drops quickly upon heating when these weak intermolecular forces are overcome. For optical and photonic applications such as IR lenses, phase-change memory, and night vision systems, the "fragility index" dictates the material's processing window. The authors believe that the "covalent network" is a subset of the structure and that the overall macroscopic properties—including the glass transition—are governed by the "glue" of vdW interactions.

Acknowledgments

The authors recognized the need for this paper after many years of mutual collaboration with Dr. Kathleen A. Richardson, her students, and colleagues at the University of Central Florida, CREOL division. Dr. Richardson is one of the world's leading authorities on ChG science and has provided helpful comments and encouragement throughout our journey.

Ethical Statement

This study does not contain any studies with human or animal subjects performed by any of the authors.

Conflicts of Interest

The authors declare that they have no conflicts of interest to this work.

Data Availability Statement

Data sharing not applicable—the authors generated no new data. All elastic properties data used by the authors to develop their models, equations, and example calculations were extracted from the sources provided below [DA01-DA08] and in references [24–40]. In this regard, all data have been measured over the course of the last 20 years. In some cases, peer-reviewed journal articles for a specific glass family and/or composition's elastic properties data were not available. For reputable data sources, the authors relied on the scientific expertise of the major infrared optical chalcogenide glass manufacturing companies: Schott North America, Inc., Amorphous Materials, Inc., Vitron Spezialwerkstoffe, GmbH, and Wavelength Opto-Electronics, Singapore (using their published datasheets).

DA01. *Comparison of IR transmitting glasses produced by AMI* (Version5). https://www.amorphousmaterials.com/app/download/6541860504/Comparison+of+IR+Materials+ver+5.pdf

DA02. Schott. (2025). *IRG25 datasheet*. https://www.schott.com/en-us/products/infrared-glasses-and-materials/downloads

DA03. Schott. (2025). *IRG22 datasheet*. https://www.schott.com/en-us/products/infrared-glasses-and-materials/downloads

DA04. Schott. (2025). *IRG27 datasheet*. https://www.schott.com/en-us/products/infrared-glasses-and-materials/downloads

DA05. Vitron. (2025). *IG-2 datasheet*. https://www.vitron.de/upload/vitron-ig-2-datenblatt-okt-2020-1_901.pdf

DA06. Vitron. (2025). *IG-3 datasheet*. https://www.vitron.de/upload/vitron-ig-3-datenblatt-okt-2020-1_55.pdf

DA07. Hilton, A. R., Hayes, D. J., & Rechtin, M. D. (1974). *Chalcogenide glasses for high energy laser application* (Report No. TI-08-74-44). Texas Instruments. https://apps.dtic.mil/sti/html/tr/AD0782036/index.html

DA08. *Wavelength opto-electronic datasheets*. https://wavelength-oe.com/wp-content/uploads/Chalcogenide-Materials.pdf

Author Contribution Statement

Richard A. Loretz: Conceptualization, Methodology, Validation, Formal analysis, Investigation, Resources, Data curation, Writing – original draft, Writing – review & editing, Visualization, Supervision, Project administration. **Thomas J. Loretz:** Formal analysis, Investigation, Resources, Writing – original draft, Writing – review & editing, Visualization, Project administration.

References

[1] Loretz, R. A., Loretz, T. J., & Richardson, K. A. (2022). Predictive method to assess chalcogenide glass properties: Bonding, density and the impact on glass properties. *Optical Materials Express*, *12*(5), 2012–2027. https://doi.org/10.1364/OME.455523

[2] Loretz, R. A., & Loretz, T. J. (2024). Modified chalcogenide glass equations for the activation energy of crystallization. *Journal of Optics and Photonics Research*, *1*(1), 16–22. https://doi.org/10.47852/bonviewJOPR42022177

[3] Singla, S., Mannan, S., Zaki, M., & Krishnan, N. M. A. (2023). Accelerated design of chalcogenide glasses through interpretable machine learning for composition–property relationships. *Journal of Physics: Materials*, *6*(2), 024003. https://doi.org/10.1088/2515-7639/acc6f2

[4] Jung, G., Alkemade, R. M., Bapst, V., Coslovich, D., Filion, L., Landes, F. P., . . . , & Biroli, G. (2025). Roadmap on machine learning glassy dynamics. *Nature Reviews Physics*, *7*(2), 91–104. https://doi.org/10.1038/s42254-024-00791-4

[5] Alzubaidi, L., Zhang, J., Humaidi, A. J., Al-Dujaili, A., Duan, Y., Al-Shamma, O., . . . , & Farhan, L. (2021). Review of deep learning: Concepts, CNN architectures, challenges, applications, future directions. *Journal of Big Data*, *8*(1), 53. https://doi.org/10.1186/s40537-021-00444-8

[6] Oyama, N., Koyama, S., & Kawasaki, T. (2023). What do deep neural networks find in disordered structures of glasses? *Frontiers in Physics*, *10*, 1007861. https://doi.org/10.3389/fphy.2022.1007861

[7] Jung, G., Biroli, G., & Berthier, L. (2023). Predicting dynamic heterogeneity in glass-forming liquids by physics-inspired machine learning. *Physical Review Letters*, *130*(23), 238202. https://doi.org/10.1103/PhysRevLett.130.238202

[8] Alkemade, R. M., Boattini, E., Filion, L., & Smallenburg, F. (2022). Comparing machine learning techniques for predicting glassy dynamics. *The Journal of Chemical Physics*, *156*(20), 204503. https://doi.org/10.1063/5.0088581

[9] Cassar, D. R., Santos, G. G., & Zanotto, E. D. (2021). Designing optical glasses by machine learning coupled with a genetic algorithm. *Ceramics international*, *47*(8), 10555–10564. https://doi.org/10.1016/j.ceramint.2020.12.167

[10] Bhattoo, R., Bishnoi, S., Zaki, M., & Krishnan, N. M. A. (2023). Understanding the compositional control on electrical, mechanical, optical, and physical properties of inorganic glasses with interpretable machine learning. *Acta Materialia*, *242*, 118439. https://doi.org/10.1016/j.actamat.2022.118439

[11] Kim, E. C., Chun, D. J., Park, C. B., & Sung, B. J. (2023). Machine learning predicts the glass transition of two-dimensional colloids besides medium-range crystalline order. *Physical Review E*, *108*(4), 044602. https://doi.org/10.1103/PhysRevE.108.044602

[12] Bødker, M. L., Bauchy, M., Du, T., Mauro, J. C., & Smedskjaer, M. M. (2022). Predicting glass structure by physics-informed machine learning. *npj Computational Materials*, *8*(1), 192. https://doi.org/10.1038/s41524-022-00882-9

[13] Zaki, M., Jayadeva, & Krishnan, N. M. A. (2024). Interpretable machine learning for understanding compositional and testing condition effects on refractive index, density, dielectric constant, and loss tangent of inorganic melts and glasses. *Frontiers in Materials*, *11*, 1412701. https://doi.org/10.3389/fmats.2024.1412701

[14] Armeli, G., Peters, J.-H., & Koop, T. (2023). Machine-learning-based prediction of the glass transition temperature of organic compounds using experimental data. *ACS Omega*, *8*(13), 12298–12309. https://doi.org/10.1021/acsomega.2c08146

[15] Dennis, J. M., & Zubarev, D. Y. (2021). Hebbian learning on small data enables experimental discovery of high T_g polyimides. *The Journal of Physical Chemistry A*, *125*(31), 6829–6835. https://doi.org/10.1021/acs.jpca.1c02959

[16] Zhang, T., Wang, S., Chai, Y., Yu, J., Zhu, W., Li, L., & Li, B. (2024). Prediction and interpretability study of the glass transition temperature of polyimide based on machine learning with quantitative structure–property relationship (T_g-QSPR). *The Journal of Physical Chemistry B*, *128*(36), 8807–8817. https://doi.org/10.1021/acs.jpcb.4c00756

[17] Forrest, R. M., & Greer, A. L. (2022). Machine-learning improves understanding of glass formation in metallic systems. *Digital Discovery*, *1*(4), 476–489. https://doi.org/10.1039/d2dd00026a

[18] Bobadilla, R. D. B., Baricco, M., & Palumbo, M. (2025). Machine learning-driven prediction of glass-forming ability in Fe-based bulk metallic glasses using thermophysical features and data augmentation. *Metals*, *15*(7), 763. https://doi.org/10.3390/met15070763

[19] Ren, B., Long, Z., & Deng, R. (2021). A new criterion for predicting the glass-forming ability of alloys based on machine learning. *Computational Materials Science*, *189*, 110259. https://doi.org/10.1016/j.commatsci.2020.110259

[20] Lu, X., Weller, Z. D., Gervasio, V., & Vienna, J. D. (2024). Glass design using machine learning property models with prediction uncertainties: Nuclear waste glass formulation. *Journal of Non-Crystalline Solids*, *631*, 122907. https://doi.org/10.1016/j.jnoncrysol.2024.122907

[21] Ghorbani, A., Askari, A., Malekan, M., & Nili-Ahmadabadi, M. (2022). Thermodynamically-guided machine learning modelling for predicting the glass-forming ability of bulk metallic glasses. *Scientific Reports*, *12*(1), 11754. https://doi.org/10.1038/s41598-022-15981-2

[22] Belciu, M.-I., & Velea, A. (2025). Ensemble machine learning for the prediction and understanding of the refractive index in chalcogenide glasses. *Molecules*, *30*(8), 1745. https://doi.org/10.3390/molecules30081745

[23] Danewalia, S. S., & Singh, K. (2025). An improved machine learning strategy using structural features to predict the glass transition temperature of oxide glasses. *Digital Discovery*, *4*(12), 3764–3773. https://doi.org/10.1039/D5DD00326A

[24] Wang, T. (2015). *Investigations on structure and properties of Ge-As-Se chalcogenide glasses*. [Doctoral dissertation, The Australian National University]. Australian National University Open Research Repository. https://doi.org/10.25911/5d70f03451201

[25] Hilton, A. R. (2010). *Chalcogenide glasses for infrared optics*. McGraw-Hill.

[26] El-Mallawany, R. A. H. (2014). *Tellurite glasses handbook: Physical properties and data*. CRC Press.

[27] Hewak, D., Bastock, P., Craig, C., Huang, C. C., Khan, K., Ravagli, A., & Weatherby, E. (2016). Next generation chalcogenide glasses for visible and IR imaging. In *SPIE Security + Defence and Remote Sensing Conference*, *401683*.

[28] Gueguen, Y., Sangleboeuf, J.-C., Keryvin, V., Rouxel, T., King, E. A., Robin, E., . . . , & Lucas, P. (2008). Sub-T_g viscoelastic behaviour of chalcogenide glasses, anomalous viscous flow and stress relaxation. *Journal of the Ceramic Society of Japan*, *116*(1356), 890–895. https://doi.org/10.2109/jcersj2.116.890

[29] Giridhar, A., Mahadevan, S., & Singh, A. K. (1984). Elastic properties of As-Sb-Se glasses. *Bulletin of Materials Science*, *6*(6), 1001–1007. https://doi.org/10.1007/BF02743948

[30] Hewak, D. W., Brady, D., Curry, R. J., Elliott, G., Huang, C. C., Hughes, M., . . . , & Sproat, C. (2010). Chalcogenide glasses for photonics device applications. In G. S. Murugan (Ed.), *Photonic glasses and glass-ceramics* (pp. 29–102). Research Signpost.

[31] Yang, G., Gueguen, Y., Sangleboeuf, J.-C., Rouxel, T., Boussard-Plédel, C., Troles, J., . . . , & Bureau, B. (2013). Physical properties of the Ge_xSe_{1-x} glasses in the 0 <x< 0.42 range in correlation with their structure. *Journal of Non-Crystalline Solids*, *377*, 54–59. https://doi.org/10.1016/j.jnoncrysol.2013.01.049

[32] Lonergan, J., Lonergan, C., McCloy, J., & Richardson, K. A. (2019). Modeling and experimental determination of physical properties of Ge_x-Ga_y-Se_{1-x-y} chalcogenide glasses I: Structure and mechanical properties. *Journal of Non-Crystalline Solids*, *510*, 192–199. https://doi.org/10.1016/j.jnoncrysol.2019.01.031

[33] Rouxel, T. (2007). Elastic properties and short-to medium-range order in glasses. *Journal of the American Ceramic Society*, *90*(10), 3019–3039. https://doi.org/10.1111/j.1551-2916.2007.01945.x

[34] Guin, J.-P., Rouxel, T., Sangleboeuf, J.-C., Melscoët, I., & Lucas, J. (2002). Hardness, toughness, and scratchability of germanium–selenium chalcogenide glasses. *Journal of the American Ceramic Society*, *85*(6), 1545–1552. https://doi.org/10.1111/j.1151-2916.2002.tb00310.x

[35] Shchurova, T. N., & Savchenko, N. D. (2001). Correlation between mechanical parameters for amorphous chalcogenide films. *Journal of Optoelectronics and Advanced Materials*, *3*(2), 491–498.

[36] Raj Adhikari, D., Adhikari, S. K., & Lamichhane, H. P. (2019). Study of thermodynamic parameter and elastic constants in lead chalcogenides. *International Journal of Advances in Scientific Research and Engineering*, *5*(5), 166–170. https://doi.org/10.31695/IJASRE.2019.33208

[37] Šiljegović, M. V., Skuban, F., Štrbac, G. R., Raonić, R., & Lukić-Petrović, S. R. (2021). Correlation between thermo-mechanical properties and network structure in Pb-As_2S_3 quasibinary chalcogenides. *Processing and Application of Ceramics*, *15*(4), 344–350. https://doi.org/10.2298/PAC2104344S

[38] Yang, G., Bureau, B., Rouxel, T., Gueguen, Y., Gulbiten, O., Roiland, C., . . . , & Lucas, P. (2010). Correlation between structure and physical properties of chalcogenide glasses in the As_xSe_{1-x} system. *Physical Review B, 82*(19), 195206. https://doi.org/10.1103/PhysRevB.82.195206

[39] Hilton, A. R. (1966). Nonoxide chalcogenide glasses as infrared optical materials. *Applied Optics*, *5*(12), 1877–1882. https://doi.org/10.1364/AO.5.001877

[40] Hubert, M., Calvez, L., & Zhang, X.-H. (2013). New chalcogenide glasses in the $GeSe_2$–Ga_2Se_3–In_2Se_3 and $GeSe_2$–Ga_2Se_3–PbSe domains. *Journal of Non-Crystalline Solids*, *377*, 8–11. https://doi.org/10.1016/j.jnoncrysol.2013.02.005

How to Cite: Loretz, R. A., & Loretz, T. J. (2026). Estimator Algorithms for Determining the Elastic Properties of Chalcogenide Glasses Based on Elemental Composition. *Journal of Optics and Photonics Research*. https://doi.org/10.47852/bonviewJOPR62028736